



20 **ABSTRACT:** The particle mixing state plays a significant yet poorly quantified role
21 in aerosol radiative forcing, especially for the mixing of dust (mineral absorbing) and
22 anthropogenic pollution (black carbon absorbing) over East Asia. We have
23 investigated the absorption enhancement of mixed-type aerosols over East Asia by
24 using the Aerosol Robotic Network observations and radiative transfer model
25 calculations. The mixed-type aerosols exhibit significantly enhanced absorbing ability
26 than the corresponding unmixed dust and anthropogenic aerosols, as revealed in the
27 spectral behavior of absorbing aerosol optical depth, single scattering albedo, and
28 imaginary refractive index. The aerosol radiative efficiencies for the dust, mixed-type,
29 and anthropogenic aerosols are -101.0 , -112.9 and $-98.3 \text{ Wm}^{-2} \tau^{-1}$ at the bottom of the
30 atmosphere (BOA), -42.3 , -22.5 and $-39.8 \text{ Wm}^{-2} \tau^{-1}$ at the top of the atmosphere
31 (TOA), and 58.7 , 90.3 and $58.5 \text{ Wm}^{-2} \tau^{-1}$ in the atmosphere (ATM), respectively. The
32 BOA cooling and ATM heating efficiencies of the mixed-type aerosols are
33 significantly higher than those of the unmixed aerosol types over the East Asia region,
34 resulting in atmospheric stabilization. In addition, the mixed-type aerosols correspond
35 to a lower TOA cooling efficiency, indicating that the cooling effect by the
36 corresponding individual aerosol components is partially counteracted. We conclude
37 that the interaction between dust and anthropogenic pollution not only represents a
38 viable aerosol formation pathway but also results in unfavorable dispersion conditions,
39 both exacerbating the regional air pollution in East Asia. Our results highlight the
40 necessity to accurately account for the mixing state of aerosols in atmospheric models
41 over East Asia, in order to better understand the formation mechanism for regional air
42 pollution and to assess its impacts on human health, weather, and climate.

43



44 **1 Introduction**

45 Atmospheric aerosols or particulate matter (PM) profoundly affect the energy
46 budget of the earth-atmosphere system directly by interfering with the radiative
47 transfer and indirectly by modifying cloud formation (Twomey, 1977; Charlson and
48 Schwartz, 1992; Fan et al., 2007; Wang et al., 2011). However, the assessment of the
49 aerosol radiative effects is limited because of the inherent difficulties associated with
50 observations and model simulations (Stevens and Bony, 2013; Kok et al., 2017). In
51 particular, an accurate quantification of the mixing state of absorbing aerosols poses a
52 great challenge in the estimation of the aerosol direct radiative forcing (Haywood and
53 Boucher, 2000; He et al., 2015). Currently, the assessment of the aerosol direct and
54 indirect radiative forcing represents large uncertainty in the prediction of future
55 climate by anthropogenic activities (IPCC, 2007; IPCC, 2013). Moreover, aerosol
56 mixing state significantly affects atmospheric dynamics (Ramanathan and Carmichael,
57 2008).

58 Atmospheric aerosols are typically internally and/or externally mixed during
59 their lifetimes (Jacobson, 2001; Zhang and Zhang, 2005; Zhang et al., 2008; Khalizov
60 et al., 2009a; Pagels et al., 2009; Taylor et al., 2015). The East Asian region is
61 experiencing persistent heavy air pollution conditions in the present day (Guo et al.,
62 2014; Zhang et al., 2015; Wang et al., 2016). Black carbon (BC) is one of the major
63 anthropogenic pollutants in this region that exerts significant environmental and
64 climatic effects because of the strong absorption of solar radiation (Wang et al., 2012;
65 Peng et al., 2016). East Asia is also the largest dust source region second to the
66 Saharan Desert (Huang et al., 2014; Huang et al., 2015; Tian et al., 2015). As a result,
67 coarse mode dust particles are frequently mixed with anthropogenic pollution along
68 their transport pathway in East Asia (Noh et al., 2012; Logan et al., 2013; Guo et al.,



69 2017; Hara et al., 2017). The potential anthropogenic influence on dust has been
70 investigated close to the dust source regions (Huang et al., 2010; Bi et al., 2017).
71 Lower single scattering albedo (SSA) of mixed dust plumes has been assessed in
72 previous studies (Kim et al., 2005; Khatri et al., 2014). Li et al. (2015) have studied
73 the SSA spectral curvature of the East Asian aerosol mixtures using Aerosol Robotic
74 Network (AERONET) products and model simulations. The observations from a
75 sun–sky radiometer and a lidar have been applied to identify the presence of Asian
76 dust in mixed aerosol plumes at several East Asian monitoring sites (Noh et al., 2017).
77 Those earlier studies on optical properties and radiative effects of the East Asian dust
78 and anthropogenic aerosol mixtures have promised reduction of the uncertainties in
79 estimating the aerosol radiative effects.

80 Internal mixing of coarse mode dust with fine mode anthropogenic aerosols has
81 been suggested by observations in the Asian Aerosol Characterization Experiment
82 (ACE-Asia) (Seinfeld et al., 2004) and recent studies (Sugimoto et al., 2015; Wang et
83 al., 2017), although the mechanism leading to the mixing has yet to be elucidated.
84 Internal mixing of dust with anthropogenic pollution likely occurs via condensation of
85 low-volatility organic and inorganic compounds, particle-phase reactions, and
86 coagulation with other aerosol types (Zhang et al., 1996; Zhao et al., 2006; Qiu et al.,
87 2011). In addition, dust particles provide reactive surfaces for catalytic conversion of
88 sulfur dioxide to sulfate, which has been suggested as a key mechanism for severe
89 haze formation in China (Zhang et al., 2015; Li et al., 2017a). Atmospheric
90 measurements using electron microscopy have identified BC and certain soluble
91 aerosols on the surface of dust particles (Tobo et al., 2010; Ma et al., 2012; Li et al.,
92 2014). Pan et al. (2017) have studied the morphology change of East Asian dust
93 mixing with anthropogenic aerosols and showed the possibility evidence for the



94 occurrence of aqueous-phase reactions.

95 The aerosol mixing state significantly affects the radiative effects (Jacobson,
96 2001; Khalizov et al., 2009b; Xue et al., 2009). Several previous studies have shown
97 that the amount of solar radiation reaching the Earth surface through mixtures of
98 mineral dust and other absorbing aerosols is considerably reduced compared to that
99 through dust-only aerosols (Derimian et al. 2008; Obregón et al. 2015). Researchers
100 have reported that the radiative efficiency of non-dust aerosols is higher than that of
101 dust aerosols at two urban Asian cities of Gwangju and Beijing (Noh et al., 2012; Yu
102 et al., 2016). Maximum radiative efficiency under unpolluted conditions has been
103 found by comparing aerosol radiative effects under different air quality conditions
104 (Chen et al., 2016). Aerosol radiative efficiency has been found to be strongly
105 influenced by aerosol absorbing ability (e.g., SSA) and size of fine mode particles in
106 Central China (Zhang et al., 2017).

107 Although the mixing state of dust and anthropogenic aerosols considerably
108 affects aerosol radiative effects, the radiative absorption enhancement by the aerosol
109 mixtures in East Asia has not been assessed. In this present work, we have extensively
110 investigated the radiative absorption enhancement by the East Asian aerosol mixtures
111 on the basis of long-term AERONET observations and SBDART model simulations.
112 We classified the dust, mixed-type, and anthropogenic aerosols according to the
113 aerosol SSA spectral behavior and Ångström exponent parameter. The optical and
114 microphysical properties of the various aerosol types were analyzed, with emphasis
115 on the absorption enhancement by mixed-type aerosols. The mechanism leading to the
116 radiative absorption enhancement by the mixed-type aerosols and their impacts on
117 regional air pollution and climate have been discussed. Our results suggest that the
118 East Asian aerosol mixtures result in a more stable atmosphere that is unfavorable for



119 diffusion and dispersion of the atmospheric pollutants.

120 **2 Data and methodology**

121 **2.1 AERONET data**

122 The aerosol optical and microphysical data used in this research were originally
123 from the Aerosol Robotic Network (AERONET) (Holben et al., 1998). To ensure the
124 data quality, we only analyzed the cloud-screened, quality-assured Level 2.0 inversion
125 data. We further constrained the data with solar zenith angle between 50° and 80° to
126 avoid possible inversion errors and surface albedo smaller than 0.5 to exclude
127 seasonal snow-covered surfaces. The AERONET spectral products are available at the
128 wavelengths of 440, 675, 870, and 1020 nm, respectively. Previously, Dubovik et al.
129 (2000) have evaluated the uncertainty of the AERONET products.

130 All available worldwide measurement sites from the Aerosol Robotic Network
131 (AERONET) program with a sample number of greater than 100 were included in the
132 present work. Considering the regional representativeness and data availability, 11
133 sites (Table S1 and Fig. S1) were selected to represent the various types of the East
134 Asian aerosol mixtures. For example, the sample numbers of Beijing and Xianghe
135 were randomly reduced to a one-fourth of the total numbers because these two sites
136 are close to each other and the total sample numbers of the two sites are significantly
137 larger than the others.

138 **2.2 Radiative forcing and efficiency calculations**

139 The aerosol direct radiative forcing (ΔF) is defined as follows:

$$140 \quad \Delta F = (F^\downarrow - F^\uparrow) - (F_0^\downarrow - F_0^\uparrow) \quad (1)$$

141 where F and F_0 are radiative fluxes under the aerosol-free and aerosol-laden
142 conditions respectively, the upward and downward arrows denote the directions of the
143 radiative fluxes. The AERONET products include the aerosol radiative forcing and



144 efficiency, in addition to the optical and microphysical parameters. However, the
145 radiative forcing in the AERONET products was not exactly calculated using
146 Equation (1). Instead, we calculated the aerosol direct radiative forcing and efficiency
147 by using the widely adopted Santa Barbara DISORT Atmospheric Radiative Transfer
148 (SBDART) model (Ricchiazzi et al., 1998). The aerosol radiative efficiency (ΔF^{eff}) is
149 defined as the aerosol direct radiative forcing per unit aerosol optical depth (AOD):

$$150 \quad \Delta F^{eff} = \Delta F / AOD_{0.55} \quad (2)$$

151 where $AOD_{0.55}$ is the 550 nm AOD. However, the aerosol direct radiative forcing is
152 not linearly dependent on AOD (e.g., Wu et al., 2015). To exclude possible errors
153 from aerosol loading in calculating the aerosol radiative efficiency in Equation (2), the
154 550 nm AOD was set to unity ($AOD_{0.55}=1.0$) in SBDART model calculations. The data
155 processing procedure is presented in Fig. 1 and a detailed discussion of aerosol
156 radiative forcing and efficiency calculation has been provided elsewhere (Tian et al.,
157 2018).

158 **2.3 Aerosol classification**

159 The SSA spectral behavior and the Ångström exponent parameter were applied
160 to identify aerosol mixtures (Fig. 1). The main absorbing component of the
161 anthropogenic pollutants is BC, which exhibits strong absorption throughout a broad
162 wavelength range (Bond and Bergstrom, 2006). Dust aerosols are also an absorbing
163 medium because of the iron-bearing minerals such as hematite, goethite and magnetite,
164 which enable the dust aerosols to absorb strongly in the UV and short visible
165 wavelengths and weakly in the near infrared (Schuster et al., 2016). Thus, the dust
166 aerosols exhibit a monotonically increasing SSA trend with increasing wavelength,
167 while the anthropogenic pollutants (the absorption of which is mainly contributed by
168 BC) show a monotonically decreasing SSA spectra (Bergstrom et al., 2007; Giles et



169 al., 2012; Tian et al., 2017). The absorption of aerosol mixtures is contributed by both
170 dust and BC, leading to a non-monotonic SSA spectra (Khatri et al., 2014). The
171 characteristic non-monotonic SSA spectral behavior of mixed-type aerosols provides
172 a useful approach to identify the mixed-type aerosols. SSA curvature of greater than
173 0.1, which has been suggested for “moderate mixing” (Li et al., 2015), was applied
174 for the mixed-type aerosol. We employed an additional criterion, Ångström exponent,
175 which is related to the aerosol size and the widely used in aerosol classification (Eck
176 et al., 2010; Derimian et al., 2016), to further constrain the aerosol classification.
177 Results show that Ångström exponent values are smaller for coarse mode dust
178 aerosols (lower than 0.7 in the present study), larger for fine mode anthropogenic
179 aerosols (greater than 1.4 in this research), and range from 0.8 and 1.3 for the
180 mixed-type aerosols, respectively.

181 The imaginary refractive index at 440 nm (k_{440} , in the visible bands) versus the
182 average of the imaginary refractive indices at 675, 870, and 1020 nm (k_{mir} , in the red
183 and near-infrared bands) is shown in Fig. 2. Anthropogenic aerosols with the
184 absorption mainly contributed by BC particles exhibit a flat imaginary refractive
185 index (Bond and Bergstrom, 2006), while dust with the components such as hematite
186 absorbs strongly in UV but weakly in longer wavelengths (Hsu and Matijević, 1985;
187 Schuster et al., 2016). Hence, the data of anthropogenic aerosols are scattered along
188 the 1:1 line (Fig. 2). Dust aerosols show stronger absorption at the visible wavelength
189 than at the red and near-infrared wavelengths, so the data are scattered above the 1:1
190 line. The data for most of the mixed-type aerosols lie above the 1:1 line and on the
191 right side of the $k_{mir} = 0.0042$ threshold, which is suggested by Schuster et al. (2016)
192 to separate dust ($k_{mir} < 0.0042$) and biomass burning ($k_{mir} > 0.0042$) aerosols. The



193 mixed-type aerosols show the strongest absorption and most of the sites with a
194 mixed-type aerosol sample number of 50 and higher are located in East Asia. Hence,
195 our method quantitatively separated various aerosol types.

196 **3 Spectral behavior of the East Asian aerosol mixtures**

197 Extensive investigations of the spectral optical properties were carried out to
198 discuss the enhanced absorbing ability of the East Asian aerosol mixtures. Dust
199 aerosols show the highest spectral AOD and the anthropogenic aerosols exhibit the
200 lowest spectral AOD (Fig. 3a). The spectral dependence of dust aerosols is nearly
201 invariant across the wavelength spectrum while the dependence of anthropogenic
202 aerosols is relatively high, which is relevant to aerosol size and the Ångström
203 parameter (Ångström, 1929). The mixed-type aerosols have smaller AOD than dust
204 aerosols, but higher absorption aerosol optical depth (AAOD) throughout the
205 wavelength band of 440 to 1020 nm (Fig. 3b). Dust aerosols exhibit higher AAOD at
206 the 440 nm wavelength than that of anthropogenic aerosols.

207 As expected by using our SSA spectral classification method, dust aerosols show
208 a monotonic increasing SSA trend with increasing wavelength, while anthropogenic
209 aerosols exhibit an opposite trend. In contrast, the SSA of the mixed-type aerosols
210 peaks at the wavelength of 675 nm (Fig. 3c). Interestingly, the mixed-type aerosols
211 exhibit the lowest SSA value that cannot be predicted by our classification method
212 because the classification method considers the spectral trend rather than the value of
213 SSA. This indicates enhanced absorption for the mixed-type aerosols. The spectral
214 average SSA of the dust, mixed-type, and anthropogenic aerosols are 0.94, 0.89, and
215 0.93, respectively. Hence, internal mixing of the East Asian aerosol mixtures yields
216 the lowest SSA that is distinct from the corresponding individual aerosol types.

217 The dust aerosols exhibit the highest value for the real part of the complex



218 refractive index, while the anthropogenic aerosols show the lowest value (Fig. 3e).
219 Interestingly, the real refractive index of the mixed-type aerosols is close to that of
220 dust aerosols, indicating high scattering of the mixed-type aerosols. The spectral
221 imaginary refractive index for anthropogenic aerosols is nearly constant (Fig. 3f),
222 which is characteristic of this aerosol type. However, the imaginary refractive index
223 of anthropogenic aerosols is much lower than that of BC aerosols (approximately 0.6
224 in Bond and Bergstrom (2006)), because the majority of anthropogenic aerosol
225 components are non-absorbing aerosols such as sulfate and nitrate salts. The spectral
226 imaginary refractive index of dust aerosols is similar to the AERONET dust
227 climatology over Africa and the Middle East (Schuster et al., 2016), with stronger
228 absorption at the visible wavelength (440 nm). The mixed-type aerosols exhibit the
229 highest imaginary refractive index, especially at the visible wavelength, where the
230 imaginary refractive index of the mixed-type aerosols (0.0159) is more than twice that
231 of anthropogenic aerosols (0.0078).

232 Hence, the absorbing ability of the East Asian aerosols is significantly enhanced
233 due to the mixing process, in light of the lowest SSA and the highest AOD and
234 imaginary refractive index for the mixed-type aerosols.

235 **4 Enhanced radiative absorption by East Asian aerosol mixtures**

236 To investigate the radiative effects caused by the enhanced absorbing ability of
237 the East Asian aerosol mixtures, we calculated the average aerosol direct radiative
238 efficiency at the bottom of the atmosphere (BOA), at the top of the atmosphere (TOA),
239 and in the atmosphere (ATM) (Fig. 4), respectively. The mixed-type aerosols exhibit
240 lower spectral average AOD (0.48) than dust aerosols (0.64) (Fig. 4a), but show
241 comparable radiative forcing relative to dust aerosols at BOA (-72.7 and -73.6 Wm^{-2}
242 for the mixed-type and dust aerosols, respectively) (Fig. 4a). This feature is explained



243 by higher BOA cooling efficiency of the mixed-type aerosols ($-112.9 \text{ Wm}^{-2}\tau^{-1}$) than
244 dust ($-101.0 \text{ Wm}^{-2}\tau^{-1}$) (Fig. 4b). The radiative absorption enhancement is evident for
245 the TOA and ATM forcing: the mixed-type aerosols exhibit the highest ATM radiative
246 forcing (55.0 Wm^{-2}) and the lowest absolute TOA forcing (-17.8 Wm^{-2}). For
247 comparison, we calculated the aerosol radiative efficiency of various aerosol types to
248 rule out the effect of aerosol loading. The mixed-type aerosols exhibit the highest
249 BOA cooling efficiency, the highest ATM heating efficiency ($90.3 \text{ Wm}^{-2}\tau^{-1}$), and the
250 lowest TOA cooling efficiency ($-22.5 \text{ Wm}^{-2}\tau^{-1}$).

251 The average BOA radiative efficiency of dust aerosols ($-101.0 \text{ Wm}^{-2}\tau^{-1}$) in the
252 present study (Fig. 4b) falls in the range of -96.1 to $-127.0 \text{ Wm}^{-2}\tau^{-1}$ by Yu et al. (2016),
253 but lower than the result of $-124.6 \pm 12.2 \text{ Wm}^{-2}\tau^{-1}$ by Noh et al. (2012). Note that
254 results by Noh et al. (2012) and Yu et al. (2016) are likely biased due to a non-linear
255 dependence between aerosol direct radiative forcing and AOD, which is avoided in
256 the present study. Our previous work (Tian et al., 2018), which used the same
257 radiative efficiency calculation method but a different aerosol classification approach
258 from the present study, obtained a similar BOA radiative efficiency of $-102.3 \text{ Wm}^{-2}\tau^{-1}$
259 at the Semi-Arid Climate and Environment Observatory of Lanzhou University
260 (SACOL), Northwest China.

261 The spatial distributions of the aerosol radiative efficiency for BOA, ATM, and
262 TOA are presented in Figs. 5-7, respectively. Only those sites with a sample number
263 of greater than 50 were averaged and included in the figures. Despite the fact that
264 AERONET sites are unavailable in some remote areas, the worldwide aerosol
265 distributions are well captured by the AERONET observations. The mixed-type
266 aerosols are distributed in East Asia, India and around the Saharan Desert regions.

267 The mixed-type aerosols exhibit a higher BOA radiative cooling efficiency than



268 that of dust and anthropogenic aerosols over the East Asia region (Fig. 5). The BOA
269 radiative cooling efficiency over India is also high, but the difference of various
270 aerosol types is small. Biomass burning aerosols over Africa exhibit the highest BOA
271 cooling efficiency in the globe, which may be explained by the different combustion
272 compositions and processes as described in Eck et al. (2010) and Garc á et al. (2012).
273 Anthropogenic aerosols over North America and dust aerosols around the Sahara
274 Desert show a relatively lower BOA cooling efficiency.

275 The mixed-type aerosols also exhibit a higher ATM radiative heating efficiency
276 than dust and anthropogenic aerosols over East Asia (Fig. 6). The ATM radiative
277 heating efficiency over India is high for all aerosol types. The ATM radiative heating
278 efficiency is high over South Africa, where biomass burning aerosols dominate. On
279 the other hand, the ATM radiative heating efficiency over North America and around
280 the Sahara Desert regions is relatively smaller.

281 The enhanced BOA cooling and ATM heating efficiencies reveal that the
282 mixed-type aerosols exhibit higher BOA cooling and ATM heating effects than those
283 of the unmixed dust and anthropogenic aerosols with the same aerosol loading. The
284 enhanced BOA cooling and ATM heating effects lead to a cooler surface and warmer
285 atmosphere and restrain the development of the planetary boundary layer, resulting in
286 a more stable atmosphere that is unfavorable for dispersion of atmospheric gaseous
287 and PM pollutants. Noting that mixed-type aerosols occur frequently in East Asia and
288 their occurrence can reach as high as fifty percent over some locations (Li et al.,
289 2015). Hence, the mixed-type aerosols likely play a significant role in enhancing air
290 pollution over East Asia. In addition, the mixed-type aerosols show lower TOA
291 radiative cooling efficiency than dust and anthropogenic aerosols over the East Asia
292 region (Fig. S1). The reduced TOA cooling efficiency indicates that the East Asian



293 aerosol mixtures partially counteract the cooling effect of the Earth-atmosphere
294 system by the corresponding individual components.

295 **5 Discussions**

296 The aerosol direct radiative efficiency strongly depends on solar zenith angle
297 (e.g., Derimian et al., 2016). To investigate the influence of solar zenith angle on the
298 result of the present study, the aerosol radiative efficiency as a function of solar zenith
299 angle were calculated for various aerosol types (Fig. 7). Note that the AERONET data
300 used in the present study is only available between 50 ° to 80 ° solar zenith angles. The
301 BOA radiative cooling and ATM heating efficiencies (absolute value of radiative
302 efficiency) decrease with increasing solar zenith angle (decreasing cosine of solar
303 zenith angle), while the TOA cooling efficiency increase with increasing solar zenith
304 angle. The mixed-type aerosols exhibit higher BOA cooling efficiency, higher ATM
305 heating efficiency, and lower TOA cooling efficiency than those of unmixed dust and
306 anthropogenic aerosols. The dust aerosols exhibit both higher BOA and TOA cooling
307 efficiency than the anthropogenic aerosols, leading to small difference in the ATM
308 heating efficiency between the two aerosol types.

309 Aerosol absorption has been suggested as a key factor that determines the aerosol
310 radiative effects (Li et al., 2010). The aerosol radiative efficiencies as a function of
311 SSA and imaginary refractive index for various aerosol types were calculated to
312 investigate the effect of aerosol absorbing on the aerosols radiative efficiency (Figs. 8
313 and 9). The BOA cooling efficiency and ATM heating efficiency increase with
314 increasing absorption (i.e., decreasing SSA and increasing imaginary refractive index)
315 and the TOA cooling efficiency decrease with increasing absorption. However, the
316 dependences between radiative efficiency and SSA are stronger than those between
317 radiative efficiency and the imaginary refractive index for BOA, TOA, and ATM. The



318 dependences between radiative efficiency and SSA are approximately linear, but the
319 dependences between radiative efficiency and imaginary refractive index become less
320 apparent with increasing imaginary refractive index. The strong dependence between
321 aerosol radiative efficiency and SSA has also been shown over Central China and
322 desert and semi-desert regions of northwestern China (Xin et al., 2016; Zhang et al.,
323 2017).

324 We also examined the effects of the fraction of fine and coarse mode on aerosol
325 radiative efficiency (Fig. 10). The BOA cooling and ATM heating efficiencies (TOA
326 cooling efficiency) initially increase (decreases) with increasing fine mode fraction
327 (FMF), when FMF is lower than 0.3 and coarse mode dust aerosols dominate. Then
328 the BOA cooling and ATM heating efficiencies (TOA cooling efficiency) reach a peak
329 (bottom) in the FMF range of 0.3 to 0.5. Finally the BOA cooling and ATM heating
330 efficiency (TOA cooling efficiency) begin to decrease (increase) when FMF is greater
331 than 0.5, where fine mode anthropogenic aerosols become dominate. Overall, the
332 moderate mixing of dust with fine mode anthropogenic pollutants, which is classified
333 as mixed-type aerosols in the present study, is responsible for the enhanced radiative
334 absorption. A previous study (Li et al., 2015) has revealed that moderate mixing of
335 East Asian dust with fine mode pollutants is responsible for high SSA spectral
336 curvature, which suggests well-mixed aerosol mixtures.

337 **6 Conclusions**

338 The mixing state of atmospheric aerosols plays a significant yet poorly
339 quantified role in determining the aerosol optical properties and radiative effects. In
340 the East Asia region, coarse mode dust and fine mode anthropogenic pollution are
341 typically mixed externally and/or internally in the atmosphere. The mixing of dust
342 with anthropogenic aerosols exerts a significant influence on aerosol absorption and



343 radiative efficiency. We present an extensive investigation of the radiative effects of
344 the East Asian aerosol mixtures.

345 The mixed-type aerosols exhibit significantly higher AAOD, lower SSA, and
346 higher imaginary refractive index than those of unmixed dust and anthropogenic
347 aerosols, showing significantly enhanced absorption. The absorption enhancement is
348 most evident at wavelength 440 nm, where the imaginary refractive index of the
349 mixed-type aerosols (0.0159) is more than twice that of anthropogenic aerosols
350 (0.0078). The mixed-type aerosols also exhibit a unique non-monotonic SSA trend,
351 which provides a characteristic signature for identifying these aerosols.

352 The values of the aerosol radiative efficiencies for dust, mixed-type and
353 anthropogenic aerosols are -101.0 , -112.9 and $-98.3 \text{ Wm}^{-2}\tau^{-1}$ for BOA, -42.3 , -22.5
354 and $-39.8 \text{ Wm}^{-2}\tau^{-1}$ for TOA, and 58.7 , 90.3 and $58.5 \text{ Wm}^{-2}\tau^{-1}$ for ATM, respectively.
355 The mixed-type aerosols exhibit significantly higher BOA radiative cooling efficiency
356 and ATM heating efficiency than those of dust and anthropogenic aerosols over East
357 Asia. These enhanced BOA cooling and ATM heating efficiencies reveal that the
358 mixed-type aerosols exhibit stronger BOA cooling and ATM heating effects than
359 those of unmixed dust and anthropogenic aerosols for a given aerosol loading,
360 resulting in a more stable atmosphere that is unfavorable for the diffusion and
361 dispersion of the gaseous and PM pollution. Hence, our results suggest that the
362 mixed-type aerosols likely play a significant role in enhancing the air pollution in East
363 Asia, because the mixing of dust and anthropogenic aerosols occurs frequently in this
364 region. In addition, the mixed-type aerosols show lower TOA cooling efficiency,
365 indicating that the mixed-type aerosols partially counteract the cooling effect of the
366 earth-atmosphere system by the corresponding individual components. Since dust
367 particles play a catalytic role in the conversion of sulfur dioxide to sulfate (Zhang et



368 al., 2015; Li et al., 2017a), the interaction between dust and anthropogenic aerosols
369 also provides a possible mechanism for the observed efficient internal mixing and
370 enhanced radiative absorption over East Asia.

371 Multiple factors have been suggested to be responsible for severe air pollution in
372 East Asia, including the interaction between BC aerosols and the atmospheric
373 boundary layer (Ding et al., 2016; Peng et al., 2016; Li et al., 2017b), rapid secondary
374 aerosol formation during severe haze events (Wang et al., 2016), weakening of the
375 East Asian monsoon circulation (Wu et al., 2016), and climate change (Cai et al,
376 2017). Our results indicate that interaction between dust and anthropogenic pollution
377 does not only represent a plausible pathway for PM formation and internal mixing but
378 also results in unfavorable dispersion conditions (i.e., increased atmospheric stability),
379 both exacerbating regional air pollution in East Asia. Clearly, future studies are
380 necessary to more accurately assess the mixing state of aerosols in atmospheric
381 models, in order to better understand the formation mechanism for air pollution over
382 East Asian and to assess its impacts on human health, weather, and climate (Zhang et
383 al., 2015).

384 **7 Data availability**

385 The original sun photometer data are available from the AERONET website
386 (<http://aeronet.gsfc.nasa.gov/>). The radiative flux data for the worldwide AERONET
387 sites calculated using the SBDART model and all data for the figures and table in the
388 present research are available from the authors upon request.

389 **Competing interests.** The authors declare that they have no conflict of interest.

390 **Acknowledgements.** This research was financially supported by National Natural
391 Science Foundation of China (41627807 and 41475008) and National Key R&D



392 Program of China (2016YFC0401003). Yuan Wang acknowledged the support from
393 NASA ROSES ACPMAP. Yuemeng Ji was financially supported by National Natural
394 Science Foundation of China (41675122) and Science and Technology Program of
395 Guangzhou city (201707010188). The authors thank the principal investigators and
396 staff for establishing and maintaining the AERONET sites used in this research. We
397 thank Institute for Computational Earth System Science (ICESS), University of
398 California for providing the SADART model. Y. Wang, J.H. Jiang, and Y.L. Yung
399 acknowledge support by the Jet Propulsion Laboratory, California Institute of
400 Technology, under contract with NASA.

401 **References**

- 402 Ångström, A.: On the Atmospheric Transmission of Sun Radiation and on Dust in the
403 Air, *Geografiska Annaler*, 11, 156-166, doi:10.2307/519399, 1929.
- 404 Bergstrom, R. W., Pilewskie, P., Russell, P. B., Redemann, J., Bond, T. C., Quinn, P.
405 K., and Sierau, B.: Spectral absorption properties of atmospheric aerosols, *Atmos.*
406 *Chem. Phys.*, 7, 5937-5943, doi:10.5194/acp-7-5937-2007, 2007.
- 407 Bi, J., Huang, J., Shi, J., Hu, Z., Zhou, T., Zhang, G., Huang, Z., Wang, X., and Jin, H.:
408 Measurement of scattering and absorption properties of dust aerosol in a Gobi
409 farmland region of northwestern China – a potential anthropogenic influence,
410 *Atmos. Chem. Phys.*, 17, 7775-7792, doi:10.5194/acp-17-7775-2017, 2017.
- 411 Bond, T. C., and Bergstrom, R. W.: Light Absorption by Carbonaceous Particles: An
412 Investigative Review, *Aerosol Sci. Tech.*, 40, 27-67,
413 doi:10.1080/02786820500421521, 2006.
- 414 Cai, W., Li, K., Liao, H., Wang, H., and Wu, L.: Weather conditions conducive to
415 Beijing severe haze more frequent under climate change, *Nat. Clim. Change*, 7,
416 257-262, doi:10.1038/nclimate3249, 2017.
- 417 Charlson, R. J., Schwartz, S. E., Hales, J. M., Cess, R. D., Coakley, J. A., Hansen, J.
418 E., and Hofmann, D. J.: Climate Forcing by Anthropogenic Aerosols, *Science*, 255,
419 423-430, doi:10.1126/science.255.5043.423, 1992.
- 420 Chen, W., Tang, H., Zhao, H., and Yan, L.: Analysis of Aerosol Properties in Beijing
421 Based on Ground-Based Sun Photometer and Air Quality Monitoring Observations



- 422 from 2005 to 2014, *Remote Sens.*, 8, 110, 2016.
- 423 Derimian, Y., León, J. F., Dubovik, O., Chiapello, I., Tanré D., Sinyuk, A., Auriol, F.,
424 Podvin, T., Brogniez, G., and Holben, B. N.: Radiative properties of aerosol
425 mixture observed during the dry season 2006 over M'Bour, Senegal (African
426 Monsoon Multidisciplinary Analysis campaign), *J. Geophys. Res.-Atmos.*, 113,
427 D00C09, doi:10.1029/2008JD009904, 2008.
- 428 Derimian, Y., Dubovik, O., Huang, X., Lapyonok, T., Litvinov, P., Kostinski, A. B.,
429 Dubuisson, P., and Ducos, F.: Comprehensive tool for calculation of radiative
430 fluxes: illustration of shortwave aerosol radiative effect sensitivities to the details in
431 aerosol and underlying surface characteristics, *Atmos. Chem. Phys.*, 16, 5763-5780,
432 doi:10.5194/acp-16-5763-2016, 2016.
- 433 Ding, A. J., Huang, X., Nie, W., Sun, J. N., Kerminen, V. M., Petäjä T., Su, H., Cheng,
434 Y. F., Yang, X. Q., Wang, M. H., Chi, X. G., Wang, J. P., Virkkula, A., Guo, W. D.,
435 Yuan, J., Wang, S. Y., Zhang, R. J., Wu, Y. F., Song, Y., Zhu, T., Zilitinkevich, S.,
436 Kulmala, M., and Fu, C. B.: Enhanced haze pollution by black carbon in megacities
437 in China, *Geophys. Res. Lett.*, 43, 2873-2879, doi:10.1002/2016GL067745, 2016.
- 438 Dubovik, O., and King, M. D.: A flexible inversion algorithm for retrieval of aerosol
439 optical properties from Sun and sky radiance measurements, *J. Geophys.*
440 *Res.-Atmos.*, 105, 20673-20696, doi:10.1029/2000JD900282, 2000.
- 441 Eck, T. F., Holben, B. N., Sinyuk, A., Pinker, R. T., Goloub, P., Chen, H., Chatenet, B.,
442 Li, Z., Singh, R. P., Tripathi, S. N., Reid, J. S., Giles, D. M., Dubovik, O., O'Neill,
443 N. T., Smirnov, A., Wang, P., and Xia, X.: Climatological aspects of the optical
444 properties of fine/coarse mode aerosol mixtures, *J. Geophys. Res.-Atmos.*, 115,
445 D19205, doi:10.1029/2010JD014002, 2010.
- 446 Fan, J., Zhang, R., Li, G., and Tao, W. K.: Effects of aerosols and relative humidity on
447 cumulus clouds, *J. Geophys. Res.-Atmos.*, 112, D14204, 2007.
- 448 García, O. E., Díaz, J. P., Expósito, F. J., Díaz, A. M., Dubovik, O., Derimian, Y.,
449 Dubuisson, P., and Roger, J. C.: Shortwave radiative forcing and efficiency of key
450 aerosol types using AERONET data, *Atmos. Chem. Phys.*, 12, 5129-5145,
451 doi:10.5194/acp-12-5129-2012, 2012.
- 452 Giles, D. M., Holben, B. N., Eck, T. F., Sinyuk, A., Smirnov, A., Slutsker, I.,
453 Dickerson, R. R., Thompson, A. M., and Schafer, J. S.: An analysis of AERONET
454 aerosol absorption properties and classifications representative of aerosol source



- 455 regions, *J. Geophys. Res.-Atmos.*, 117, D17203, doi:10.1029/2012JD018127, 2012.
- 456 Guo, J., Lou, M., Miao, Y., Wang, Y., Zeng, Z., Liu, H., He, J., Xu, H., Wang, F., and
457 Min, M.: Trans-Pacific transport of dust aerosols from East Asia: Insights gained
458 from multiple observations and modeling, *Environ. Pollut.*, 230, 1030-1039, 2017.
- 459 Guo, S., Hu, M., Zamora, M. L., Peng, J., Shang, D., Zheng, J., Du, Z., Wu, Z., Shao,
460 M., Zeng, L., Molina, M. J., and Zhang, R.: Elucidating severe urban haze
461 formation in China, *P. Natl. Acad. Sci. USA*, 111, 17373-17378,
462 doi:10.1073/pnas.1419604111, 2014.
- 463 Hara, Y., Nishizawa, T., Sugimoto, N., Matsui, I., Pan, X., Kobayashi, H., Osada, K.,
464 and Uno, I.: Optical properties of mixed aerosol layers over Japan derived with
465 multi-wavelength Mie–Raman lidar system, *J. Quant. Spectrosc. Ra.* 188, 20-27,
466 2017.
- 467 Haywood, J., and Boucher, O.: Estimates of the direct and indirect radiative forcing
468 due to tropospheric aerosols: A review, *Rev. Geophys.*, 38, 513-543, 2000.
- 469 He, C., Liou, K. N., Takano, Y., Zhang, R., Zamora, M. L., Yang, P., Li, Q., and Leung,
470 L. R.: Variation of the radiative properties during black carbon aging: theoretical
471 and experimental intercomparison, *Atmos. Chem. Phys. Discuss.*, 15, 19835-19872,
472 doi:10.5194/acpd-15-19835-2015, 2015.
- 473 Holben, B. N., Eck, T. F., Slutsker, I., Tanré D., Buis, J. P., Setzer, A., Vermote, E.,
474 Reagan, J. A., Kaufman, Y. J., Nakajima, T., Lavenu, F., Jankowiak, I., and Smirnov,
475 A.: AERONET—A Federated Instrument Network and Data Archive for Aerosol
476 Characterization, *Remote Sens. Environ.*, 66, 1-16, 1998.
- 477 Hsu, W. P., and Matijević, E.: Optical properties of monodispersed hematite hydrosols,
478 *Appl. Optics*, 24, 1623-1630, doi:10.1364/AO.24.001623, 1985.
- 479 Huang, J., Wang, T., Wang, W., Li, Z., and Yan, H.: Climate effects of dust aerosols
480 over East Asian arid and semiarid regions, *J. Geophys. Res.-Atmos.*, 119,
481 11,398-311,416, doi:10.1002/2014JD021796, 2014.
- 482 Huang, K., Zhuang, G., Li, J., Wang, Q., Sun, Y., Lin, Y., and Fu, J. S.: Mixing of
483 Asian dust with pollution aerosol and the transformation of aerosol components
484 during the dust storm over China in spring 2007, *J. Geophys. Res.-Atmos.*, 115,
485 D00K13, doi:10.1029/2009JD013145, 2010.
- 486 Huang, Z., Huang, J., Hayasaka, T., Wang, S., Zhou, T., and Jin, H.: Short-cut
487 transport path for Asian dust directly to the Arctic: a case study, *Environ. Res. Lett.*,



- 488 10, 114018, 2015.
- 489 IPCC, 2007: Climate Change 2007: The Physical Science Basis. Contribution of
490 Working Group I to the Fourth Assessment Report of the Intergovernmental Panel
491 on Climate Change [Solomon, S., D. Qin, M. Manning, Z. Chen, M. Marquis, K.B.
492 Averyt, M. Tignor and H.L. Miller (eds.)]. Cambridge University Press, Cambridge,
493 United Kingdom and New York, NY, USA, 996 pp.
- 494 IPCC, 2013: Climate Change 2013: The Physical Science Basis. Contribution of
495 Working Group I to the Fifth Assessment Report of the Intergovernmental Panel on
496 Climate Change [Stocker, T.F., D. Qin, G.-K. Plattner, M. Tignor, S.K. Allen, J.
497 Boschung, A. Nauels, Y. Xia, V. Bex and P.M. Midgley (eds.)]. Cambridge
498 University Press, Cambridge, United Kingdom and New York, NY, USA, 1535 pp.
- 499 Jacobson, M. Z.: Strong radiative heating due to the mixing state of black carbon in
500 atmospheric aerosols, *Nature*, 409, 695-697, 2001.
- 501 Khalizov, A. F., Zhang, R., Zhang, D., Xue, H., Pagels, J., and Mcmurry, P. H.:
502 Formation of highly hygroscopic soot aerosols upon internal mixing with sulfuric
503 acid vapor, *J. Geophys. Res.-Atmos.*, 114, D05208, 2009a.
- 504 Khalizov, A. F., Xue, H., Wang, L., Zheng, J., and Zhang, R.: Enhanced Light
505 Absorption and Scattering by Carbon Soot Aerosol Internally Mixed with Sulfuric
506 Acid, *J. Phys. Chem. A*, 113, 1066-1074, 2009b.
- 507 Khatri, P., Takamura, T., Shimizu, A., and Sugimoto, N.: Observation of low single
508 scattering albedo of aerosols in the downwind of the East Asian desert and urban
509 areas during the inflow of dust aerosols, *J. Geophys. Res.-Atmos.*, 119, 787-802,
510 doi:10.1002/2013JD019961, 2014.
- 511 Kim, D.-H., Sohn, B. J., Nakajima, T., and Takamura, T.: Aerosol radiative forcing
512 over east Asia determined from ground-based solar radiation measurements, *J.*
513 *Geophys. Res.-Atmos.*, 110, D10S22, doi:10.1029/2004JD004678, 2005.
- 514 Kok, J. F., Ridley, D. A., Zhou, Q., Miller, R. L., Zhao, C., Heald, C. L., Ward, D. S.,
515 Albani, S., and Haustein, K.: Smaller desert dust cooling effect estimated from
516 analysis of dust size and abundance, *Nat. Geosci.*, 10, 274-278,
517 doi:10.1038/ngeo2912, 2017.
- 518 Li, G., Bei, N., Cao, J., Huang, R., Wu, J., Feng, T., Wang, Y., Liu, S., Zhang, Q., and
519 Tie, X.: A possible pathway for rapid growth of sulfate during haze days in China,
520 *Atmospheric Chemistry & Physics*, 17, 1-43, 2017a.



- 521 Li, J., Carlson, B. E., and Lacis, A. A.: Using single-scattering albedo spectral
522 curvature to characterize East Asian aerosol mixtures, *J. Geophys. Res.-Atmos.*,
523 120, 2037-2052, doi:10.1002/2014JD022433, 2015.
- 524 Li, W., Shao, L., Shi, Z., Chen, J., Yang, L., Yuan, Q., Yan, C., Zhang, X., Wang, Y.,
525 Sun, J., Zhang, Y., Shen, X., Wang, Z., and Wang, W.: Mixing state and
526 hygroscopicity of dust and haze particles before leaving Asian continent, *J.*
527 *Geophys. Res.-Atmos.*, 119, 1044-1059, doi:10.1002/2013JD021003, 2014.
- 528 Li, Z., Lee, K.-H., Wang, Y., Xin, J., and Hao, W.-M.: First observation-based
529 estimates of cloud-free aerosol radiative forcing across China, *J. Geophys.*
530 *Res.-Atmos.*, 115, D00K18, doi:10.1029/2009JD013306, 2010.
- 531 Li, Z., Guo, J., Ding, A., Liao, H., Liu, J., Sun, Y., Wang, T., Xue, H., Zhang, H. and
532 Zhu, B.: Aerosol and Boundary-Layer Interactions and Impact on Air Quality,
533 *National Science Review*, doi:10.1093/nsr/nwx117, 2017b.
- 534 Logan, T., Xi, B., Dong, X., Li, Z., and Cribb, M.: Classification and investigation of
535 Asian aerosol absorptive properties, *Atmos. Chem. Phys.*, 13, 2253-2265,
536 doi:10.5194/acp-13-2253-2013, 2013.
- 537 Ma, Q., Liu, Y., Liu, C., Ma, J., and He, H.: A case study of Asian dust storm particles:
538 Chemical composition, reactivity to SO₂ and hygroscopic properties, *J. Environ.*
539 *Sci.*, 24, 62-71, 2012.
- 540 Noh, Y., Müller, D., Lee, H., Lee, K., Kim, K., Shin, S., and Kim, Y. J.: Estimation of
541 radiative forcing by the dust and non-dust content in mixed East Asian pollution
542 plumes on the basis of depolarization ratios measured with lidar, *Atmos. Environ.*,
543 61, 221-231, 2012.
- 544 Noh, Y., Müller, D., Lee, K., Kim, K., Lee, K., Shimizu, A., Kim, S. W., Sano, I., and
545 Park, C. B.: Depolarization ratios retrieved by AERONET sun-sky radiometer data
546 and comparison to depolarization ratios measured with lidar, *Atmos. Chem. Phys.*,
547 17, 6271-6290, doi:10.5194/acp-17-6271-2017, 2017.
- 548 Obregón, M. A., Pereira, S., Salgueiro, V., Costa, M. J., Silva, A. M., Serrano, A., and
549 Bortoli, D.: Aerosol radiative effects during two desert dust events in August 2012
550 over the Southwestern Iberian Peninsula, *Atmos. Res.*, 153, 404-415, 2015.
- 551 Pagels, J., Khalizov, A. F., McMurry, P. H., and Zhang, R. Y.: Processing of Soot by
552 Controlled Sulphuric Acid and Water Condensation—Mass and Mobility
553 Relationship, *Aerosol Sci. Tech.*, 43, 629-640, 2009.



- 554 Pan, X., Uno, I., Wang, Z., Nishizawa, T., Sugimoto, N., Yamamoto, S., Kobayashi,
555 H., Sun, Y., Fu, P., Tang, X., and Wang, Z.: Real-time observational evidence of
556 changing Asian dust morphology with the mixing of heavy anthropogenic pollution,
557 *Sci. Rep.*, 7, 335, doi:10.1038/s41598-017-00444-w, 2017.
- 558 Peng, J., Hu, M., Guo, S., Du, Z., Zheng, J., Shang, D., Levy Zamora, M., Zeng, L.,
559 Shao, M., Wu, Y.-S., Zheng, J., Wang, Y., Glen, C. R., Collins, D. R., Molina, M. J.,
560 and Zhang, R.: Markedly enhanced absorption and direct radiative forcing of black
561 carbon under polluted urban environments, *P. Natl. Acad. Sci. USA*, 113,
562 4266-4271, doi:10.1073/pnas.1602310113, 2016.
- 563 Qiu, C., Wang, L., Lal, V., Khalizov, A. F., and Zhang, R.: Heterogeneous reactions of
564 alkylamines with ammonium sulfate and ammonium bisulfate, *Environ. Sci.*
565 *Technol.*, 45, 4748-4755, 2011.
- 566 Ramanathan, V., and Carmichael, G.: Global and regional climate changes due to
567 black carbon, *Nat. Geosci.*, 1, 221-227, 2008.
- 568 Ricchiazzi, P., Yang, S. R., Gautier, C., and Sowle, D.: SBDART: A research and
569 teaching software tool for plane-parallel radiative transfer in the Earth's
570 atmosphere, *B. Am. Meteorol. Soc.*, 79, 2101-2114, doi
571 10.1175/1520-0477(1998)079<2101:Sarats>2.0.Co;2, 1998.
- 572 Schuster, G. L., Dubovik, O., and Arola, A.: Remote sensing of soot carbon – Part 1:
573 Distinguishing different absorbing aerosol species, *Atmos. Chem. Phys.*, 16,
574 1565-1585, doi:10.5194/acp-16-1565-2016, 2016.
- 575 Seinfeld, J. H., Carmichael, G. R., Arimoto, R., Conant, W. C., Brechtel, F. J., Bates, T.
576 S., Cahill, T. A., Clarke, A. D., Doherty, S. J., Flatau, P. J., Huebert, B. J., Kim, J.,
577 Markowicz, K. M., Quinn, P. K., Russell, L. M., Russell, P. B., Shimizu, A.,
578 Shinozuka, Y., Song, C. H., Tang, Y., Uno, I., Vogelmann, A. M., Weber, R. J., Woo,
579 J.-H., and Zhang, X. Y.: ACE-ASIA: Regional Climatic and Atmospheric Chemical
580 Effects of Asian Dust and Pollution, *B. Am. Meteorol. Soc.*, 85, 367-380,
581 doi:10.1175/bams-85-3-367, 2004.
- 582 Stevens, B., and Bony, S.: What Are Climate Models Missing?, *Science*, 340,
583 1053-1054, doi:10.1126/science.1237554, 2013.
- 584 Sugimoto, N., Nishizawa, T., Shimizu, A., Matsui, I., and Kobayashi, H.: Detection of
585 internally mixed Asian dust with air pollution aerosols using a polarization optical
586 particle counter and a polarization-sensitive two-wavelength lidar, *J. Quant.*



- 587 Spectrosc. Ra., 150, 107-113, 2015.
- 588 Taylor, M., Kazadzis, S., Amiridis, V., and Kahn, R. A.: Global aerosol mixtures and
589 their multiyear and seasonal characteristics, Atmos. Environ., 116, 112-129, 2015.
- 590 Tian, P., Cao, X., Zhang, L., Wang, H., Shi, J., Huang, Z., Zhou, T., and Liu, H.:
591 Observation and simulation study of atmospheric aerosol nonsphericity over the
592 Loess Plateau in northwest China, Atmos. Environ., 117, 212-219, 2015.
- 593 Tian, P., Cao, X., Zhang, L., Sun, N., Sun, L., Logan, T., Shi, J., Wang, Y., Ji, Y., Lin,
594 Y., Huang, Z., Zhou, T., Shi, Y., and Zhang, R.: Aerosol vertical distribution and
595 optical properties over China from long-term satellite and ground-based remote
596 sensing, Atmos. Chem. Phys., 17, 2509-2523, doi:10.5194/acp-17-2509-2017,
597 2017.
- 598 Tian, P., Zhang, L., Cao, X., Sun, N., Mo, X., Liang, J., Li, X., Gao, X. Zhang, B.:
599 Enhanced Bottom-of-the-Atmosphere Cooling and Atmosphere Heating Efficiency
600 by Mixed-Type Aerosols: A Classification Based on Aerosol Nonsphericity, J.
601 Atmos. Sci., 75(1), 113-124, doi: 10.1175/JAS-D-17-0019.1, 2018.
- 602 Twomey, S.: The Influence of Pollution on the Shortwave Albedo of Clouds, J Atmos
603 Sci, 34, 1149-1152, 1977.
- 604 Tobo, Y., Zhang, D., Matsuki, A., and Iwasaka, Y.: Asian dust particles converted into
605 aqueous droplets under remote marine atmospheric conditions, P. Natl. Acad. Sci.
606 USA, 107, 17905-17910, doi:10.1073/pnas.1008235107, 2010.
- 607 Wang, G., Zhang, R., Gomez, M. E., Yang, L., Levy Zamora, M., Hu, M., Lin, Y.,
608 Peng, J., Guo, S., Meng, J., Li, J., Cheng, C., Hu, T., Ren, Y., Wang, Y., Gao, J.,
609 Cao, J., An, Z., Zhou, W., Li, G., Wang, J., Tian, P., Marrero-Ortiz, W., Secret, J.,
610 Du, Z., Zheng, J., Shang, D., Zeng, L., Shao, M., Wang, W., Huang, Y., Wang, Y.,
611 Zhu, Y., Li, Y., Hu, J., Pan, B., Cai, L., Cheng, Y., Ji, Y., Zhang, F., Rosenfeld, D.,
612 Liss, P. S., Duce, R. A., Kolb, C. E., and Molina, M. J.: Persistent sulfate formation
613 from London Fog to Chinese haze, P. Natl. Acad. Sci. USA, 113, 13630-13635,
614 doi:10.1073/pnas.1616540113, 2016.
- 615 Wang, R., Tao, S., Wang, W., Liu, J., Shen, H., Shen, G., Wang, B., Liu, X., Li, W.,
616 Huang, Y., Zhang, Y., Lu, Y., Chen, H., Chen, Y., Wang, C., Zhu, D., Wang, X., Li,
617 B., Liu, W., and Ma, J.: Black Carbon Emissions in China from 1949 to 2050,
618 Environ. Sci. Technol. 46, 7595-7603, doi:10.1021/es3003684, 2012.
- 619 Wang, Y., Wan, Q., Meng, W., and Liao, F.: Long-term impacts of aerosols on



- 620 precipitation and lightning over the Pearl River Delta megacity area in China,
621 Atmos. Chem. Phys., 11, 12421-12436, 2011.
- 622 Wang, Z., Pan, X., Uno, I., Li, J., Wang, Z., Chen, X., Fu, P., Yang, T., Kobayashi, H.,
623 Shimizu, A., Sugimoto, N., and Yamamoto, S.: Significant impacts of
624 heterogeneous reactions on the chemical composition and mixing state of dust
625 particles: A case study during dust events over northern China, Atmos. Environ.,
626 159, 83-91, 2017.
- 627 Wu, G., Li, Z., Fu, C., Zhang, X., Zhang, R., Zhang, R., Zhou, T., Li, J., Li, J., Zhou,
628 D., Wu, L., Zhou, L., He, B., and Huang, R.: Advances in studying interactions
629 between aerosols and monsoon in China, Sci. China Earth Sci., 1-16,
630 doi:10.1007/s11430-015-5198-z, 2016.
- 631 Wu, Y., Zhu, J., Che, H., Xia, X., and Zhang, R.: Column-integrated aerosol optical
632 properties and direct radiative forcing based on sun photometer measurements at a
633 semi-arid rural site in Northeast China, Atmos. Res., 157, 56-65, 2015.
- 634 Xin, J., Gong, C., Wang, S., and Wang, Y.: Aerosol direct radiative forcing in desert
635 and semi-desert regions of northwestern China, Atmos. Res., 171, 56-65, 2016.
- 636 Xue, H., Khalizov, A. F., Wang, L., Zheng, J., and Zhang, R.: Effects of dicarboxylic
637 acid coating on the optical properties of soot, Phys. Chem. Chem. Phys., 11,
638 7869-7875, 2009.
- 639 Yu, X., Lü, R., Kumar, K. R., Ma, J., Zhang, Q., Jiang, Y., Kang, N., Yang, S., Wang,
640 J., and Li, M.: Dust aerosol properties and radiative forcing observed in spring
641 during 2001–2014 over urban Beijing, China, Environ. Sci. Pollut. R., 23,
642 15432-15442, doi:10.1007/s11356-016-6727-9, 2016.
- 643 Zhang, D., and Zhang, R.: Laboratory Investigation of Heterogeneous Interaction of
644 Sulfuric Acid with Soot, Environ. Sci. Technol., 39, 5722-5728,
645 doi:10.1021/es050372d, 2005.
- 646 Zhang, M., Wang, L., Gong, W., Ma, Y., and Liu, B.: Aerosol Optical Properties and
647 Direct Radiative Effects over Central China, Remote Sens., 9, 997, 2017.
- 648 Zhang, R., Mingtaun Leu, A., and Keyser, L. F.: Heterogeneous Chemistry of HONO
649 on Liquid Sulfuric Acid: A New Mechanism of Chlorine Activation on
650 Stratospheric Sulfate Aerosols, J. Phys. Chem., 100, 339-45. 1996.
- 651 Zhang, R., Khalizov, A. F., Pagels, J., Zhang, D., Xue, H., and McMurry, P. H.:
652 Variability in morphology, hygroscopicity, and optical properties of soot aerosols



653 during atmospheric processing, P. Natl. Acad. Sci. USA, 105, 10291-10296,
654 doi:10.1073/pnas.0804860105, 2008.

655 Zhang, R., Wang, G., Guo, S., Zamora, M. L., Ying, Q., Lin, Y., Wang, W., Hu, M.,
656 and Wang, Y.: Formation of Urban Fine Particulate Matter, Chem. Rev., 115,
657 3803-3855, doi:10.1021/acs.chemrev.5b00067, 2015.

658 Zhao, C., Tie, X., and Lin, Y.: A possible positive feedback of reduction of
659 precipitation and increase in aerosols over eastern central China, Geophys. Res.
660 Lett., 33, L11814, doi:10.1029/2006GL025959, 2006.

661



662

663

Figure Captions

664 **Figure 1.** Diagram of the radiative efficiency calculation and aerosol classification

665 **Figure 2.** The imaginary refractive index at 440 nm versus the average of the imaginary refractive
666 indices at 675, 870, and 1020 nm for dust, mixed-type, and anthropogenic aerosols over
667 worldwide AERONET sites. Only those sites with a sample number of 50 and higher were
668 averaged and shown in the figure.

669 **Figure 3.** Spectral behavior of (a) AOD, (b) AAOD, (c) SSA, (d) asymmetry factor, (e) real part of
670 the complex refractive index, and (f) imaginary part of the complex refractive index for dust,
671 mixed-type and anthropogenic aerosols averaged from East Asian sites.

672 **Figure 4.** (a) Radiative forcing and (b) radiative efficiency of the dust, mixed-type, and
673 anthropogenic aerosols averaged from East Asian sites.

674 **Figure 5.** Aerosol radiative efficiency at BOA: (a) dust aerosols, (b) anthropogenic aerosols, and
675 (c) mixed-type aerosols.

676 **Figure 6.** Aerosol radiative efficiency in ATM: (a) dust aerosols, (b) anthropogenic aerosols, and
677 (c) mixed-type aerosols.

678 **Figure 7.** Aerosol direct radiative efficiency as a function of the cosine of solar zenith angle for
679 the dust, mixed-type and anthropogenic aerosols: (a) BOA, (b) ATM, and (c) TOA.

680 **Figure 8.** Aerosol direct radiative efficiency as a function of SSA for the dust, mixed-type and
681 anthropogenic aerosols: (a) BOA, (b) ATM, and (c) TOA.

682 **Figure 9.** Aerosol direct radiative efficiency as a function of imaginary refractive index for the
683 dust, mixed-type and anthropogenic aerosols: (a) BOA, (b) ATM, and (c) TOA.

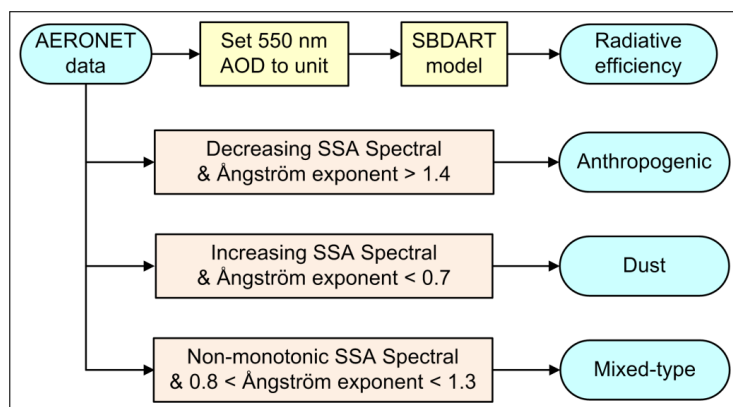
684 **Figure 10.** Aerosol direct radiative efficiency as a function of FMF in the East Asian region: (a)
685 BOA, (b) ATM, and (c) TOA. The average radiative efficiencies of the dust, mixed-type and
686 anthropogenic aerosols are also plotted.

687



688

689



690

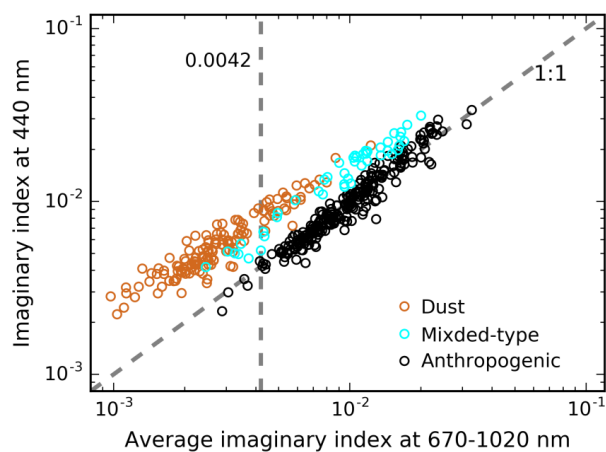
691

Figure 1. Diagram of the radiative efficiency calculation and aerosol classification

692



693



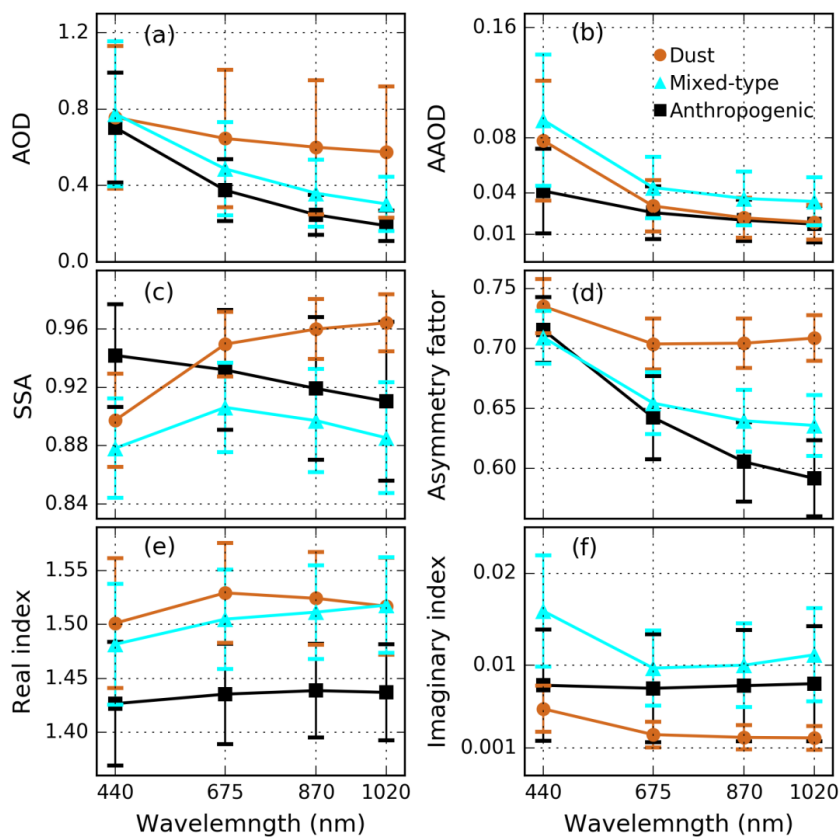
694

695 **Figure 2.** The imaginary refractive index at 440 nm versus the average of the imaginary refractive
696 indices at 675, 870, and 1020 nm for dust, mixed-type, and anthropogenic aerosols over
697 worldwide AERONET sites. Only those sites with a sample number of 50 and higher were
698 averaged and shown in the figure.

699



700



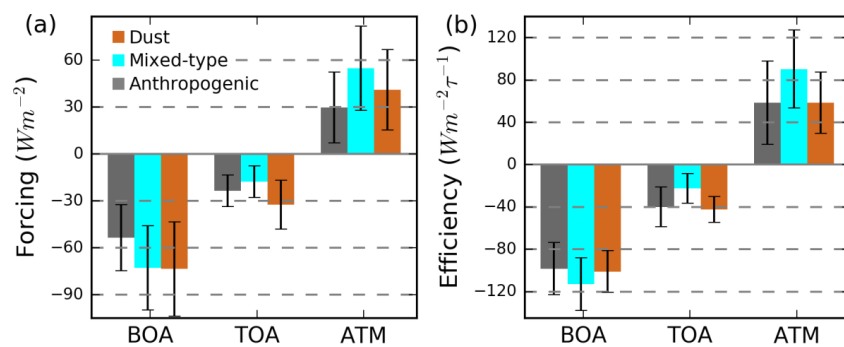
701

702 **Figure 3.** Spectral behavior of (a) AOD, (b) AAOD, (c) SSA, (d) asymmetry factor, (e) real part of
703 the complex refractive index, and (f) imaginary part of the complex refractive index for dust,
704 mixed-type and anthropogenic aerosols averaged from East Asian sites.

705



706



707

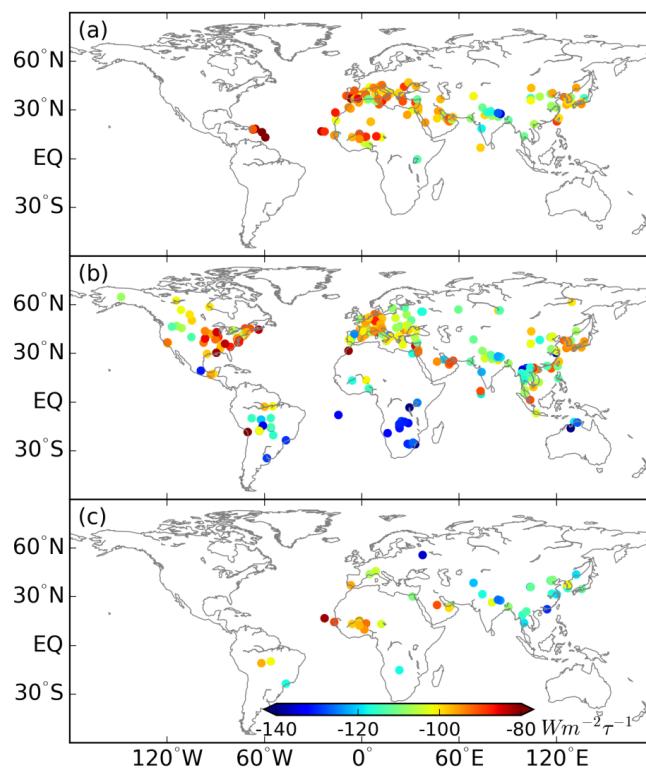
708 **Figure 4.** (a) Radiative forcing and (b) radiative efficiency of the dust, mixed-type, and

709 anthropogenic aerosols averaged from East Asian sites.

710



711



712

713 **Figure 5.** Aerosol radiative efficiency at BOA: (a) dust aerosols, (b) anthropogenic aerosols, and

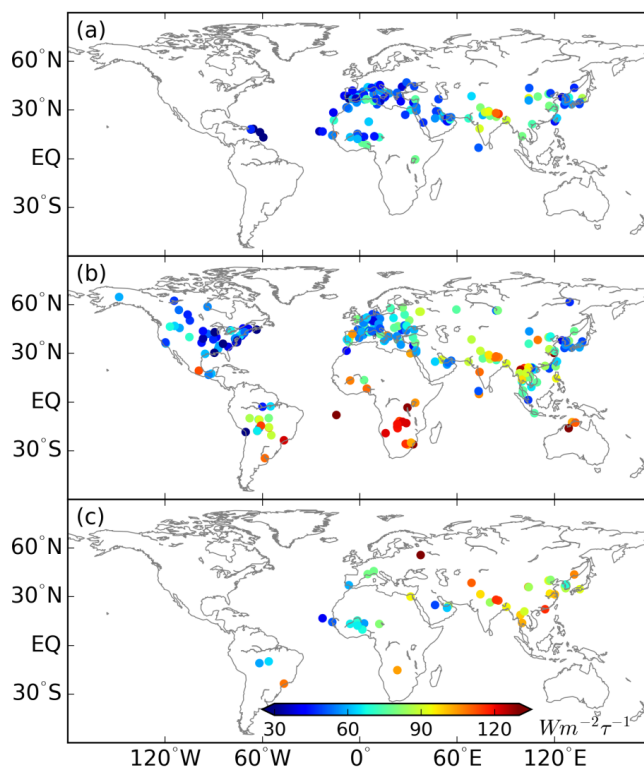
714 (c) mixed-type aerosols.

715

716



717



718

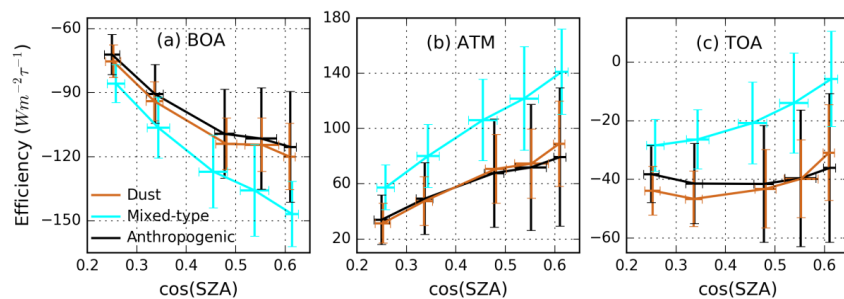
719 **Figure 6.** Aerosol radiative efficiency in ATM: (a) dust aerosols, (b) anthropogenic aerosols, and

720 (c) mixed-type aerosols.

721



722



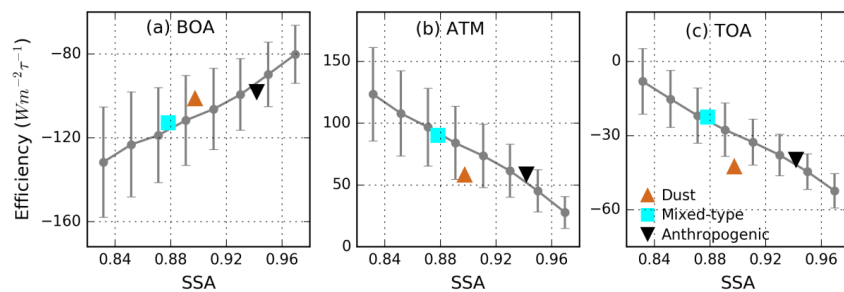
723

724 **Figure 7.** Aerosol direct radiative efficiency as a function of the cosine of solar zenith angle for
725 the dust, mixed-type and anthropogenic aerosols: (a) BOA, (b) ATM, and (c) TOA.

726



727



728

729

Figure 8. Aerosol direct radiative efficiency as a function of SSA for the dust, mixed-type and

730

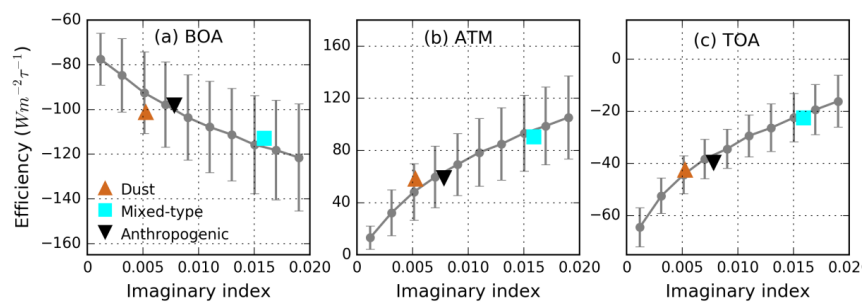
anthropogenic aerosols: (a) BOA, (b) ATM, and (c) TOA.

731

732



733



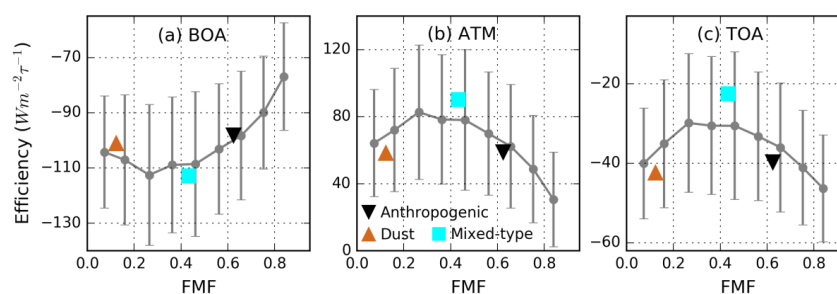
734

735 **Figure 9.** Aerosol direct radiative efficiency as a function of imaginary refractive index for the
736 dust, mixed-type and anthropogenic aerosols: (a) BOA, (b) ATM, and (c) TOA.

737



738



739

740 **Figure 10.** Aerosol direct radiative efficiency as a function of FMF in the East Asian region: (a)
741 BOA, (b) ATM, and (c) TOA. The average radiative efficiencies of the dust, mixed-type and
742 anthropogenic aerosols are also plotted.

743